# Review of Imprinted Polymer Microrings as Ultrasound Detectors: Design, Fabrication, and Characterization

Cheng Zhang, Sung-Liang Chen, Tao Ling, and L. Jay Guo, *Senior Member, IEEE*

(*Invited Paper*)

***Abstract*— Detectors play a vital role in ultrasound sensing and imaging applications. With the rapid development of photoacoustic imaging technology in recent years, novel ultrasound detectors based on optical methods have gained increased attention, among which the imprinted polymer microring is a representative one. This review covers the device design, fabrication, and characterization, with an emphasis on how the imprinting-based fabrication methodology benefits the device performance, which further facilitates photoacoustic imaging and sensing applications. By carefully designing and fabricating the imprint mold, the imprinted polymer microring has a quality factor on the order of $10^5$ at 780 nm. The device has advantages such as wide acoustic bandwidth response from dc to 350 MHz at −3 dB, low noise equivalent detectable pressure, wide acceptance angle, and so on. The polymer microring has been successfully employed in applications such as photoacoustic imaging and real-time terahertz pulse detection.**

***Index Terms*— Microring resonators, ultrasound detectors, nano-imprint, printed sensors, polymer-based photonic devices, photoacoustic imaging, real time THz detection.**

## I. Introduction

OPTICAL micro-cavity resonators have spurred much interest since the late 20th century, which now have led to numerous important applications. In 1969, Marcatili first proposed microring resonators as integrated optical wavelength filters [1]. Much investigation went into microsphere [2] and micro-droplet [3] resonators from the early 1980's to realize lasing and nonlinear optical phenomena. Microring is one of the typical forms of micro-cavity resonators, consisting of a ring shape waveguide coupled with a straight bus waveguide. It offers such advantages as high quality factor ($Q$ factor), compact size and strong optical field enhancement inside the cavities. With these characteristics, microring resonators have been demonstrated for applications in both passive and active optical devices. Passive devices include: single resonator/high-order resonator filters [4], [5], add/drop filters in wavelength division multiplexing (WDM) system [6], tunable filters [7], bio-chemical sensors [8], [9] and pressure sensors [10]–[12]. Active devices include: continuous wavelength lasers [13], [14], optical switcher/modulators [15], optical nonlinear oscillators [16], [17] and cavity based radiation pressure oscillators [18].

The materials constituting microrings can be hard materials, such as silicon [19], silicon nitride [20], silicon dioxide [21], tantalum pentoxide [22], or soft materials such as polystyrene (PS) [11], polymethylmethacrylate (PMMA) [23], SU-8 [24]–[26], to mention just a few. The structure can be fabricated through electron beam or photo lithography to define the structure directly in the polymer, or using etching method subsequently to transfer patterns into the underlying material. Etch-free selective thermal oxidation was demonstrated to fabricate high quality factor silicon microrings as well [27], [28]. Nano-imprint lithography is another effective fabrication approach, especially for polymer based structures. In nano-imprinting, a mold that contains surface-relief features is pressed into the polymeric materials cast on a substrate in a controlled condition (such as certain temperature, pressure and with ultraviolet light irradiation, etc). After their separation, a thickness contrast (complementary surface features with respect to those on the mold) will be created on the polymer material. Nano-imprinting simplifies fabrication, increases throughput and improves reproducibility. A detailed review on nano-imprinting is presented in [29].

In this review, imprinted polymer microring resonators are discussed. The device fabrication, characterization and application as ultrasound sensors are described in detail. Besides the advantages of simplified fabrication and high yield, this simple mechanical imprinting process enables highly reproducible and high quality factor polymer microring structures by using a well fabricated mold. Due to the sensitive response of the polymer materials to the acoustic pressure, the polymer microring works as a high performance ultrasound detector. It has merits such as high acoustic detection sensitivity, ultrabroad bandwidth, wide angular response and compact size, which are proved to be valuable in photoacoustic sensing and imaging applications.

Manuscript received February 12, 2015; accepted March 25, 2015. Date of publication April 10, 2015; date of current version April 22, 2015. This work was supported in part by the National Institutes of Health and in part National Science Foundation under Grant DBI-1256001. The associate editor coordinating the review of this paper and approving it for publication was Dr. Ravinder S. Dahiya.

C. Zhang and L. J. Guo are with the Department of Electrical Engineering and Computer Science, University of Michigan, Ann Arbor, MI 48109 USA (e-mail: chengzh@umich.edu; guo@umich.edu).

S.-L. Chen is with the University of Michigan—Shanghai Jiao Tong University Joint Institute, Shanghai Jiao Tong University, Shanghai 200240, China (e-mail: sungliang.chen@sjtu.edu.cn).

T. Ling is with TE Connectivity, Middletown, PA 17057 USA (e-mail: tao.ling@te.com).

Color versions of one or more of the figures in this paper are available online at http://ieeexplore.ieee.org.

Digital Object Identifier 10.1109/JSEN.2015.2421519

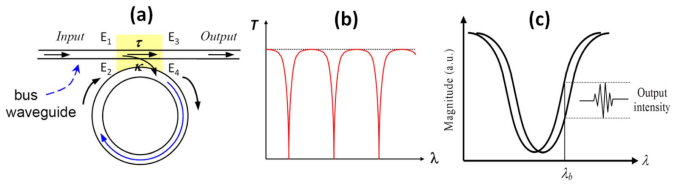


Fig. 1. (a) Schematic drawing of the microring, consisting of a ring waveguide coupled to a straight bus waveguide. (b) Transmission spectrum of the microring. (c) Ultrasound detection by the microring sensor. Reproduced with permission from [31]. Copyright 2008 IEEE.

## II. Design and Fabrication

### A. Principle

A microring resonator is composed of a ring waveguide closely coupled with a bus waveguide, as shown in figure 1a. The input and output optical fields ($E_1$ and $E_3$) in the waveguide, and the circulating optical fields in the ring ($E_2$ and $E_4$) are related to each other by the following equations [23]:

$$E_3 = \alpha\,(\tau E_1 + j\kappa E_2) \tag{1}$$

$$E_4 = \alpha\,(\tau E_2 + j\kappa E_1) \tag{2}$$

Where $\tau$ and $\kappa$ are the amplitude transmission and coupling coefficients respectively, and $\alpha$ is the insertion loss (in terms of transmission coefficient) due to the waveguide mode mismatch in the coupling region. There is a $\pi/2$ radians phase shift between the coupled fields in the ring and bus waveguide, and this is due to the general requirement from the power conservation and time reversal [30].

In the ring waveguide, the circulating fields $E_2$ and $E_4$ are related to each other by: $E_2 = a \times \exp(-j\phi) \times E_4$, where $a$ is the single-pass amplitude transmission coefficient, and $\phi$ is the single-pass accumulated phase and can be further expressed as: $\phi = (2\pi \times n_{\text{eff}} \times L)/\lambda$. Here $n_{\text{eff}}$ is the effective refractive index of the propagating mode in the ring, $L$ the ring diameter, and $\lambda$ the wavelength.

Based on the above analysis, the relation of the optical fields in the bus waveguides ($E_1$ and $E_3$) could be further expressed as:

$$E_3/E_1 = \left(\tau\alpha - a\alpha^2\left(\tau^2+\kappa^2\right)\exp(-j\phi)\right)/\left(1-\tau\alpha a\exp(-j\phi)\right) \tag{3}$$

The input and output intensity ($I_1$ and $I_3$) of the bus waveguide are related as:

$$I_3/I_1 = |E_3/E_1|^2 = \left|\left(\tau\alpha - a\alpha^2\left(\tau^2+\kappa^2\right)\exp(-j\phi)\right)/(1-\tau\alpha a\exp(-j\phi))\right|^2 \tag{4}$$

Resonance occurs when the single-pass accumulated phase $\phi$ in the ring is multiples of $2\pi(\exp(-j\phi) = 1)$. Under this condition, the output intensity is minimal (Fig. 1b). This is because $E_2$ and $E_4$ are in phase when the ring is in resonance, and therefore the optical field builds up inside the ring (constructive interference happens). However, the field coupled back to the bus waveguide has a $\pi$ radians phase difference with respect to the traveling field $E_1$ in the waveguide (thus destructive interference happens), and this leads to a minimal intensity at the output $E_3$.

The transmission amplitude is critically dependent on the phase accumulation $\phi$ inside the ring, and is thus a function of the effective refractive index ($n_{\text{eff}}$) of the propagating mode in a given ring geometry. The polymer microring is affected by the ultrasound waves in two ways: on one hand, the ring waveguide can be deformed by the acoustic pressure, which changes its shape and field distribution, thereby the $n_{\text{eff}}$ of the propagating mode; on the other hand, the polymer refractive index itself is modulated by the acoustic signal through the elastic-optic effect (Strain creates a proportional perturbation of the refractive index in the medium [32]). These two effects change the $n_{\text{eff}}$. When the probing laser wavelength is fixed at the sharpest slope of the ring resonance curve, the incoming ultrasound signal can be recorded as the time-varying output power from the microring resonator due to the resonance shift (Fig. 1c).

The sensitivity of the microring device to the acoustic pressure can be expressed as [33]:

$$S = dT/dP = (dT/d\lambda)\left(d\lambda/dn_{eff}\right)\left(dn_{eff}/dP\right) \tag{5}$$

where $T$ and $P$ are the optical transmission intensity and acoustic pressure amplitude, respectively. The first derivative $dT/d\lambda$ represents the change in the transmitted intensity with the resonance wavelength shift for a fixed probing laser wavelength. This quantity is closely related to the sharpness of the resonance curve, denoted by the $Q$ factor of the microring. The second derivative $d\lambda/dn_{eff}$ is the resonance wavelength shift with respect to the change of the effective refractive index and is a constant given the fact that the resonant wavelength shift is tiny. The third term $dn_{eff}/dP$ is a parameter signifying how sensitive the polymer properties change with respect to the ultrasonic pressure and can be described in terms of Young's modulus and elastic-optic coefficient. Therefore, the microring detector's sensitivity depends on its $Q$ factor as well as the polymer properties. It will be shown in the following discussion how we take these factors into consideration in the device design and fabrication.

### B. Fabrication

The process of the polymer microring fabrication by imprinting is schematically shown in Fig. 2a, along with the representative scanning electron micrograph (SEM) of the imprinted PS microrings (Fig. 2b). For imprinting, a good quality mold is essential. Silicon is chosen as the mold fabrication material for its wide availability and varieties of relevant fabrication processes developed by the integrated circuits (IC) industry. In particular, silicon dry etching has been demonstrated to produce vertical and smooth sidewall profiles [34], which are critical in fabricating low loss waveguides. First of all, the pattern of the microring and the bus waveguide is defined by the electron beam lithography (E-beam) on resist spun on a Si substrate. The E-beam resist is PMMA. Then the PMMA is used as the mask in plasma coupled reactive ion etching (RIE) to transfer the pattern into the Si substrate. After this, the PMMA is removed by acetone which concludes the mold fabrication process. The silicon mold is employed in a thermal imprinting process

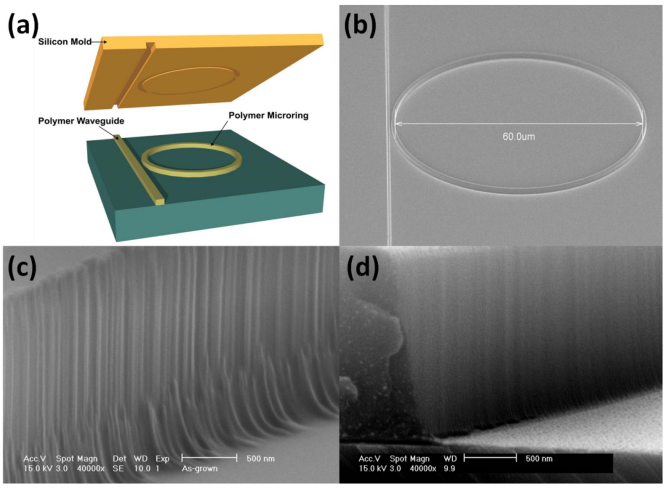


Fig. 2. (a) Polymer ring fabrication schematic by nano-imprinting lithography. (b) Angle view scanning electron microscope (SEM) of the microring with a diameter of 60 $\mu$m; Reproduced with permission from [35]. Copyright 2014 American Chemical Society. (c-d) Sidewall SEM image of the polymer micro-ring fabricated from the mold without (c) and with (d) resist reflow process and thermal oxidation during the mold fabrication. Reproduced with permission from [12]. Copyright 2011 The Optical Society of America.

on polystyrene (PS) film spun on a thermal oxide substrate (acting as the bottom cladding). PS gives better imprinting yield than PMMA [23], another popular imprinting resist. The thermal imprinting is done at 180 °C under 600 PSI pressure for 5 minutes (Nanonex NX-2000).

The roughness of the fabricated waveguide sidewalls can scatter the optical wave propagating in the waveguide and lead to the optical loss, which reduces the $Q$ factor of the microring resonators. During the imprinting, the undesired roughness on the mold sidewall is replicated onto the polymer waveguides. Although smooth sidewall of the mold is achievable by carefully controlling the silicon etching process, two more steps are developed to further reduce the sidewall roughness. The first important step is PMMA resist reflow, which is applied before the RIE to "smooth out" the line edge roughness and defects due to noise and dose variations during the E-beam process. By choosing a proper temperature and time (115 °C for 90 seconds), the reflow process can significantly reduce the imperfections in the PMMA resist and harden the edges of the PMMA pattern. Thus, there are fewer defects when transferring the pattern from PMMA into the Si substrate through RIE. After silicon etching, there is the second important step: silicon thermal oxidation followed by the buffered hydrofluoric acid (BHF) etching, where the outside layer of rough Si on the mold is converted to $SiO_2$ and subsequently removed by BHF. The oxidation is carried out in a high temperature oven and produces around 100 nm thermal oxide on the silicon surface, which is then removed by BHF. SEM pictures showing the microring sidewall profiles fabricated with molds just by etching and with both reflow and oxidation are in Figs. 2c and 2d. As an example, the $Q$ factors of devices working in the 1550 nm band are $1 \times 10^4$ and $1.1 \times 10^5$ respectively [12].

Some polymers such as PMMA and SU-8 could be directly patterned by the E-beam lithography [24], [36]. However, there are defects in the exposed polymer area, which limit device $Q$ factors in the range of $10^3$ to $10^4$. By taking an "indirect" approach, we have successfully reduced the roughness in the master silicon molds first, thereby ensuring a smooth surface profile of the polymer after imprinting. Besides, practical sensing applications call for detectors with repeatable and stable performances, which are naturally offered by the imprinting process, as the replicated structures are identical if they are imprinted by the same mold. Lastly, there are many polymers that can be patterned by imprinting as compared to the E-beam lithography. Therefore, the imprinting process is an advantageous and reliable approach to fabricate polymer microrings, as well as other polymer based photonic structures [37]–[39].

We have designed microrings working at either 1550 nm or 780 nm. 1550 nm regime is the optical communication band, and there is wide availability of finely tunable laser sources and amplifiers (e.g. Erbium doped fiber amplifier-EDFA). Device detection sensitivity is proportional to the probe laser power [40]. However, for ultrasound sensing applications, microrings are immersed in water which acts as part of the cladding medium for the ring waveguide. Water has absorption in the near-IR range due to the $-$OH bonds, which limits the device $Q$ factor. In contrast, water absorption is significantly suppressed in the shorter wavelength band, so the device working in 780 nm range enjoys $Q$ factor as high as $5.1 \times 10^5$ [11]. However, the lack of suitable/economic laser amplifiers in this frequency range, to the best of our knowledge, may limit its best sensitivity.

## III. Characterization

Fig. 2b shows the geometry of an imprinted device with working wavelength at 780 nm. The ring has a diameter of 60 $\mu$m and waveguide height of 1.4 $\mu$m. As mentioned in session 2.2, its $Q$ factor is in the order of $10^5$. The detector acoustic sensitivity is calibrated using a known acoustic source generated by a commercial ultrasound transducer [12]. One standard parameter to evaluate a detector's sensitivity is the noise-equivalent pressure (NEP), i.e. the minimum detectable acoustic pressure right above the system noise level. We have demonstrated NEPs of 10.5 Pa, 15.2 Pa and 21.4 Pa over 1-25 MHz, 1-50 MHz and 1-75 MHz respectively [11]. This is 300 times better than a similar size piezoelectric PVDF transducer (HPM 075/1, Precision Acoustics, Dorchester, Dorset, UK). We recently demonstrated an NEP of 105 Pa in the 1-350 MHz range [35]. To our knowledge, this is the first time to achieve such low noise equivalent detectable pressure in this broad bandwidth.

The ultra-broad response bandwidth is another unique property of the microring ultrasound detector [35], [41]. In photoacoustic imaging, the axial resolution is inversely proportional to the detector bandwidth (see next section). The sensor's acoustic detection bandwidth is calibrated by measuring the temporal response of the microring to a short acoustic pulse (wide bandwidth signal), generated by a 200 nm Chromium (Cr) film irradiated by a nano-second laser pulse. In the case where the laser pulse duration is far longer than the acoustic transient time across the absorber,

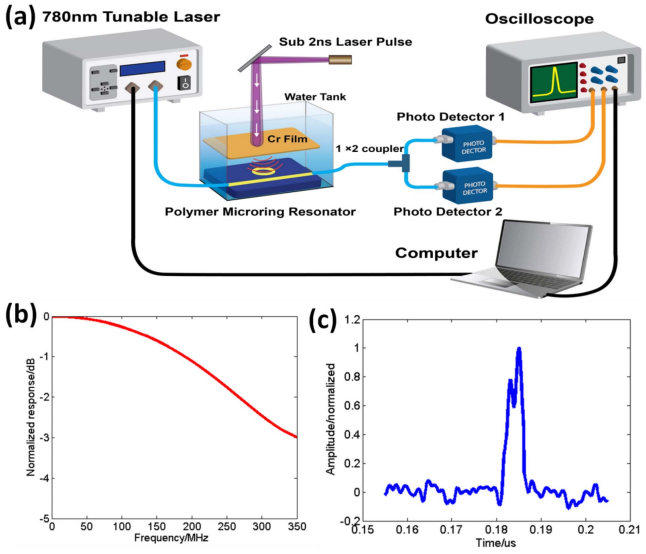


Fig. 3. (a) Experiment set-up to determine the bandwidth of the ring resonator. (b) Frequency domain ring response. The ring has −3dB bandwidth at 350 MHz. (c) Measured photoacoustic signal from two closely spaced Cr films with 1.9 ns separation in the time domain, which is a direct experimental demonstration of the super high axial resolution (2.85 $\mu$m). Reproduced with permission from [35]. Copyright 2014 American Chemical Society.

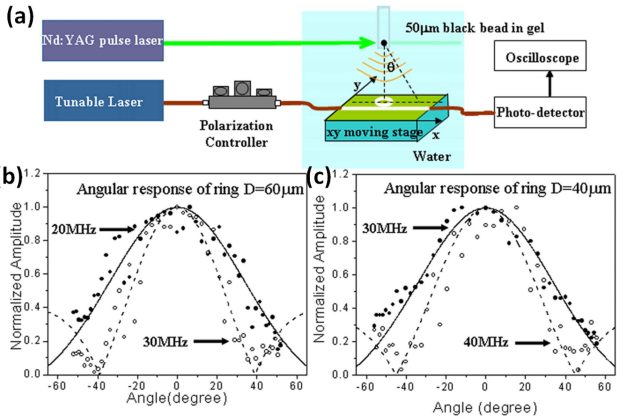


Fig. 4. (a) Experimental setup to measure the angular response of the polymer microring. (b) Experimental data (dot) and theoretical calculation (line) of angular response of the polymer microrings with $D = 60$ $\mu$m at 20 MHz (solid dot and line) and 30 MHz (empty dot and dashed line). (c) Ring with $D = 40$ $\mu$m at 30 MHz (solid dot and line) and 40 MHz (empty dot and dashed line). Reproduced with permission from [11]. Copyright 2011 AIP Publishing LLC.

the generated photoacoustic signal essentially duplicates the incident laser pulse in the time domain [42]. The experimental setup is shown in Fig. 3a. A continuous-wave (CW) 780 nm tunable laser (TLB-6312, New Focus) is fiber coupled into the device input waveguide and its output power is collected by a multimode fiber, which is connected to a $1 \times 2$ coupler with 90:10 split ratio (FCMM50-90A-FC, Thorlabs). The outputs of the coupler are detected by two photo-detectors and finally recorded by a digital oscilloscope (DSO7054A, Agilent). Ring resonance can be affected by either laser heating or other external perturbations. The change of the ring resonance wavelength will change the relative position of the probe laser wavelength on the ring resonance curve, thus affecting the device acoustic sensing property. This issue can be solved by using feedback control to "lock" the probe wavelength to a certain position of the resonance curve and choosing a ring material with good thermal stability (such as PS in our case). In this experiment, output from the 10% channel of the coupler is monitored (1601, New Focus) and used for feedback control of the tunable laser to fix its wavelength at the sharp slope of the ring resonance spectrum. While the rest 90% output is collected by a high-speed avalanche photo detector (APD210, Menlo Systems) and used for the photoacoustic signal detection. The device is immersed in de-ionized (DI) water which serves as both the top cladding of the microring and the coupling medium for the ultrasonic propagation. Fig. 3b shows the measured response bandwidth of ring. It has a flat response stretching from DC to ∼350 MHz at −3 dB (0.707). To demonstrate the high axial resolution benefited from this wide bandwidth, photoacoustic signals from two Cr films separated by a thin SU-8 spacer are measured. The films are deposited on Polyethylene terephtalate (PET) substrate, which has matched acoustic impedance with water. The detected signal is shown in figure 3c. Clearly two peaks can be distinguished with 1.9 ns separation. A 1.9 ns time domain gap translates to a 2.85 $\mu$m axial resolution in biological tissues (sound velocity 1500m/s). This value is about two folds improvement than the recent reported results [43], [44], but without any signal processing or sample treatment.

The sensor's angular sensitivity can be theoretically described by considering a ring shape transducer: $D_0 = J_0(k \times a \sin\theta)$, where $J_0$ is the zero order Bessel function of the first kind, $k$ is the wave-vector of the incident acoustic wave, $a$ is the radius of the microring and $\theta$ the incident angle of the acoustic wave. For a given $D_0$ and acoustic wave-vector $k$, smaller radius $a$ leads to a larger $\theta$ (wider angular response). The measurement set-up to characterize the ring angular sensitivity is illustrated in Fig. 4a [11]. Acoustic wave is generated from a 50 $\mu$m polystyrene black bead irradiated by a 6 ns, 532 nm pulsed laser. Microrings with diameters of 60 and 40 $\mu$m are placed about 3 mm away from the bead for signal detection. The detectors are linearly scanned to receive photoacoustic signals at different angles. Fig. 4b and 4c show the extracted angular response of different devices at different frequency bands, which agree well with theoretical calculations. The detectors have −6 dB beamwidth over 40 degrees, which benefits applications such as photoacoustic tomography and beam forming [31].

Besides the high sensitivity, broad bandwidth and wide angular response, microring sensors have other advantages such as robustness, compact size and size-independent sensitivity. These merits make microring an excellent detector for photoacoustic imaging and sensing applications. For example, the high sensitivity and broad bandwidth benefit the image resolution and signal to noise ratio (SNR) in photoacoustic microscopy [45], [46]. Its wide angular response, broad bandwidth and close-to-point detector properties make it an ideal detector in photoacoustic

TABLE I
KEY FEATURES OF IMPRINTED MICRORINGS AND THEIR COMPARISONS WITH OTHER DETECTORS

| Device | Microring | Fabry Perot polymer film detector [45] | PVDF needle hydrophone (HPM 075/1, Precision Acoustics) | Commercial transducer (V2062 Olympus NDT) |
|---|---|---|---|---|
| NEP | 105Pa over 350 MHz* | 350Pa over 20 MHz | 6 Kpa over 100 MHz | 15 Pa over 100 MHz |
| Bandwidth | DC to 350 MHz at -3 dB by measurement (estimated FWHM bandwidth to be 940 MHz) | 20 MHz | 100 MHz | 100 MHz |
| Diameter | 20-100 μm** | 50 μm | 75 μm | 3 mm |

* Measured with 60 μm diameter microring
** Acceptance angle: 40°at -6 dB beamwidth for 40 μm microring

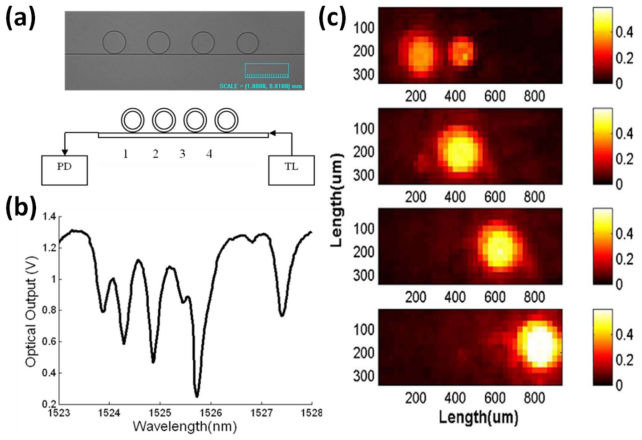


Fig. 5. (a) Optical microscopy picture of the four microring array (upper row) and the WDM scheme to probe each element (lower row). (b) Transmission spectrum measured for the array. (c) 2D spatial sensitivity of the microring array. Reproduced with permission from [31]. Copyright 2008 IEEE.

tomography [10], [47]. Its compact size facilitates applications in photoacoustic endoscopy [48]–[50]. When the microring is intergrated with terahertz (THz) absorbers such as carbon nanotubes, efficient real-time detection of terahertz pulse radiation is realized by "listening to" the generated photoacoustic signals [51], [52]. The device key features and comparisons with other detectors are summarized in Table 1.

## IV. MICRORING ARRAYS

Compared with the single element detector, sensor array has much broader applications and can speed up the image acquisition. A proof of concept experiment was done with a microring array consisting of four microrings with a single input/output waveguide (Fig. 5a) [31]. Each of them was fabricated with a slightly varying diameter, resulting in different resonant wavelengths. Therefore, each of the four elements could be addressed through the same bus waveguide by adjusting the probe laser wavelength (similar to the concept of wavelength division multiplexing-WDM). The array transmission spectrum is shown in Fig. 5b. There are more than four resonance dips, and this is because two resonances might exist for the same ring due to the presence of TE and TM modes in the ring waveguide simultaneously. However, by proper waveguide design or adjustment of input light polarization state, a cleaner spectrum can be obtained.

In order to measure the spatial sensitivity of each element, a 50 MHz $LiNbO_3$ focused ultrasound transducer with aperture diameter of 2.5 mm, focal length of 4 mm was used to insonify the microring array. The focal diameter of the transducer is approximately 50 $\mu$m. Four wavelengths were chosen corresponding to the resonant peak of each ring, and a 2D scan was performed over the entire array at each of the four wavelengths. The scanning step size was 25 $\mu$m. The waveform shape did not vary greatly between different elements although the elements with shallower resonances gave lower peak sensitivities. The spatial sensitivity of each of the four rings is shown in Fig. 5c. It can be seen that by using this "WDM" scheme, each ring gives an independent response, proving the feasibility of the array. Due to the overlap between the first two elements' resonances, a spatial scan at the resonance wavelength of the first element also displays sensitivity to the second element. But this problem can be solved by increasing the $Q$ factor of the microring and careful choice of the element size to obtain more equal resonance spacing.

To make denser arrays, smaller size rings are needed. They are also useful for high frequency ultrasonic imaging applications because of the larger angular response [47]. By using the same fabrication techniques that have been discussed in the previous section, we have fabricated $R = 20$ $\mu$m polymer microrings with reasonable $Q$ factor and sensitivity [11]. Much smaller size microring device with radius down to 10 $\mu$m has also been developed, but it suffers large leakage loss due to the low refractive index contrast between the waveguide polymer (e.g. Polystyrene n = 1.58 to 1.59) and bottom substrate silicon dioxide (n = 1.45) serving as the bottom cladding for the PS waveguide. The transmission spectrum of imprinted polymer microring is shown in the Fig. 6a and the $Q$ factor is around $4.3 \times 10^3$ in the water, translating to optical loss of about 90dB/cm.

One way to improve the device's $Q$ factor is to use higher refractive index polymer materials as waveguide core materials, such as Poly(chloro-p-xylene) (n = 1.63), Poly(vinyl phenyl sulfide) (n = 1.66), Poly(N-vinyl carbazole) (n = 1.69). They have high glass transition temperatures (above 180 °C), which require high temperature in the thermal nano-imprinting process [29]. Since it is difficult to achieve a relatively thick film (e.g. above 500 nm) by normal spin coating method because of the low dissolution rate of these polymers in solvents, conventional waveguide fabrication process, such as photolithography combined with a dry etching process, may not be feasible. In this case, imprinting process is a preferred fabrication technique as the starting polymer film layer can be much thinner than the final waveguide thickness. Another alternative approach is to reduce the refractive

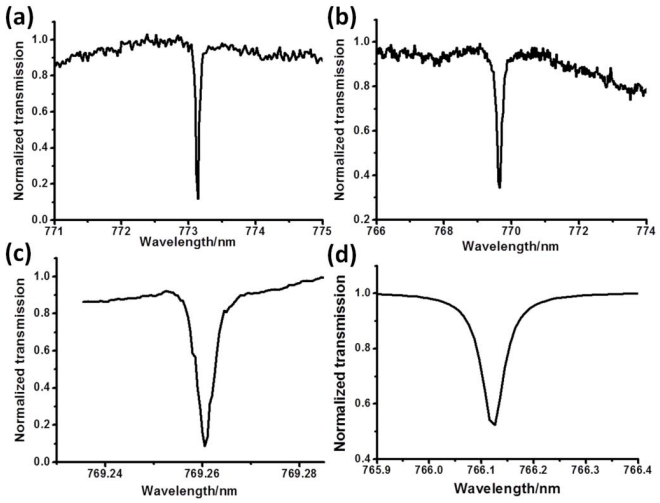


Fig. 6. (a-b) The transmission spectrum of polymer microrings with R = 10 $\mu$m on thermal oxide substrate without (a) and with (b) 400 nm thick HSQ film in the water. (c-d) Transmission spectrum of $R = 10$ $\mu$m polymer microring on the silicon substrate coated with a metal film and a 400 nm HSQ buffer layer in the air (c) and in the water (d).

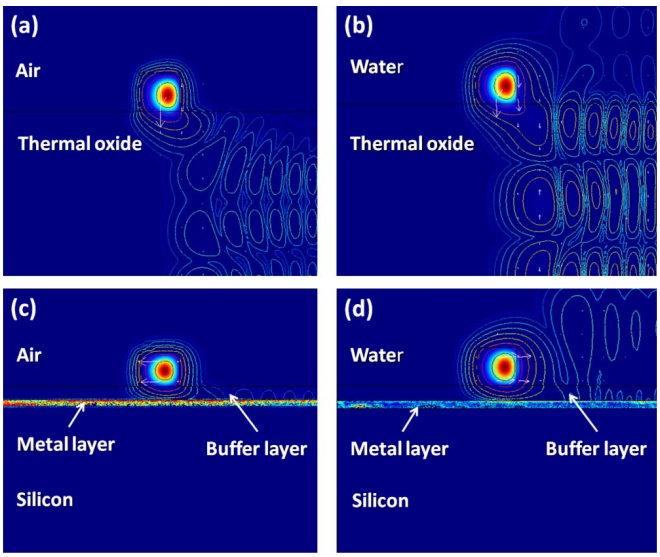


Fig. 7. (a-b) Simulated the field distribution of $R = 10$ $\mu$m polymer microring on the thermal oxide substratein air (a) and water (b); (c-d) Simulated the field distribution of $R = 10$ $\mu$m polymer microring on the silicon substrate coated with a metal film and a 400 nm HSQ buffer layer in air (c) and water (d).

index on the under-cladding layer on the substrate instead of using high index waveguide cores. A couple of low refractive index materials were studied, including hydrogen silsesquioxane (HSQ) (n = 1.40), Cytop (n = 1.34), silsesquioxane (SSQ) (n = 1.42). HSQ was chosen in our work, because of its stable property after thermally cured. The transmission spectrum of $R = 10$ $\mu$m polymer microring fabricated on substrate with 400 nm HSQ film coated on top of 4 $\mu$m thick thermal oxide is shown in the Fig. 6b, and the $Q$ factor of the device in the water can reach $2 \times 10^4$, which is 4-5 time higher than the one without the lower index HSQ film.

Another effective way to reduce the small device's bending loss is to hybrid the polymer device with a metallic substrate. The principle can be illustrated with simulation results showing the reduced radiation loss into the substrate with the help of a thin metal layer (Fig. 7). A low index thin buffer layer (such as HSQ) can be added between the waveguide material and metal to reduce the loss by the metal film. The transmission spectrum of $R = 10$ $\mu$m polymer microring on the silicon substrate with a metal film and a 400 nm low index buffer layer has been measured in the air and in the water, respectively (Figs. 7c and 7d). The device $Q$ factor is around $2 \times 10^5$ in the air and the around $2 \times 10^4$ in the water, which matched well with the simulation results from the COMSOL multi physics software. This interesting finding also suggests that the high $Q$ microring devices can be fabricated on various substrates such as flexible plastic films, metal foils or blocks and in fact any types of substrates, which opens up much broader applications.

## V. Conclusion

High $Q$ polymer microring resonators are fabricated through the imprinting process by using a pre-fabricated mold with smooth side-walls. The device high $Q$ factor (on the order of $10^5$) contributes to its sensitive acoustic response (noise equivalent detectable pressure of 105 Pa from 1-350 MHz). At the same time, its miniature size ensures ultra-broad bandwidth (from DC to 350 MHz at $-3$ dB) and wide angular response ($-6$ dB beam width over 40 degree for rings of 40 $\mu$m diameter). In addition, the detector has other merits such as robustness of operation, immunity to electromagnetic interference, etc. Integrating the rings into sensor arrays further expedites the imaging speed and this is facilitated by fabricating small size rings (e.g. 10 $\mu$m in radius) on either low refractive index or metallic substrates. Application of the detector in photoacoustic imaging system leads to improved imaging quality: e.g. faithful image reconstruction in photoacoustic tomography and high resolution in photoacoustic microscopy. Integrating the microring with other electromagnetic wave absorbers enables a broader range of photoacoustic sensing, such as real time THz pulse detection. Other novel applications will likely be developed in the future by using these characteristics.

## Acknowledgment

The authors would like to acknowledge the support by the NSF (DBI-1256001).

## References

[1] E. A. J. Marcatili, "Bends in optical dielectric guides," *Bell Syst. Tech. J.*, vol. 48, no. 7, pp. 2103–2132, 1969.
[2] R. E. Benner, P. W. Barber, J. F. Owen, and R. K. Chang, "Observation of structure resonances in the fluorescence spectra from microspheres," *Phys. Rev. Lett.*, vol. 44, pp. 475–478, Feb. 1980.
[3] S.-X. Qian, J. B. Snow, H.-M. Tzeng, and R. K. Chang, "Lasing droplets: Highlighting the liquid-air interface by laser emission," *Science*, vol. 231, pp. 486–488, Jan. 1986.
[4] B. E. Little, S. T. Chu, H. A. Haus, J. Foresi, and J.-P. Laine, "Microring resonator channel dropping filters," *J. Lightw. Technol.*, vol. 15, no. 6, pp. 998–1005, Jun. 1997.
[5] S. T. Chu, B. E. Little, W. Pan, T. Kaneko, and Y. Kokubun, "Second-order filter response from parallel coupled glass microring resonators," *IEEE Photon. Technol. Lett.*, vol. 11, no. 11, pp. 1426–1428, Nov. 1999.
[6] S. T. Chu, B. E. Little, W. Pan, T. Kaneko, S. Sato, and Y. Kokubun, "An eight-channel add–drop filter using vertically coupled microring resonators over a cross grid," *IEEE Photon. Technol. Lett.*, vol. 11, no. 6, pp. 691–693, Jun. 1999.

[7] D. Dai, L. Yang, and S. He, "Ultrasmall thermally tunable microring resonator with a submicrometer heater on Si nanowires," *J. Lightw. Technol.*, vol. 26, no. 6, pp. 704–709, Mar. 15, 2008.

[8] C.-Y. Chao and L. J. Guo, "Biochemical sensors based on polymer microrings with sharp asymmetrical resonance," *Appl. Phys. Lett.*, vol. 83, no. 8, pp. 1527–1529, 2003.

[9] I. M. White, H. Oveys, and X. Fan, "Liquid-core optical ring-resonator sensors," *Opt. Lett.*, vol. 31, no. 9, pp. 1319–1321, May 2006.

[10] S.-L. Chen, S.-W. Huang, T. Ling, S. Ashkenazi, and L. J. Guo, "Polymer microring resonators for high-sensitivity and wideband photoacoustic imaging," *IEEE Trans. Ultrason., Ferroelectr., Freq. Control*, vol. 56, no. 11, pp. 2482–2491, Nov. 2009.

[11] T. Ling, S.-L. Chen, and L. J. Guo, "High-sensitivity and wide-directivity ultrasound detection using high Q polymer microring resonators," *Appl. Phys. Lett.*, vol. 98, no. 20, p. 204103, 2011.

[12] T. Ling, S.-L. Chen, and L. J. Guo, "Fabrication and characterization of high Q polymer micro-ring resonator and its application as a sensitive ultrasonic detector," *Opt. Exp.*, vol. 19, no. 2, pp. 861–869, Jan. 2011.

[13] J. D. B. Bradley *et al.*, "Monolithic erbium- and ytterbium-doped microring lasers on silicon chips," *Opt. Exp.*, vol. 22, no. 10, pp. 12226–12237, May 2014.

[14] A. Chiasera *et al.*, "Spherical whispering-gallery-mode microresonators," *Laser Photon. Rev.*, vol. 4, no. 3, pp. 457–482, 2010.

[15] V. Van *et al.*, "All-optical nonlinear switching in GaAs-AlGaAs microring resonators," *IEEE Photon. Technol. Lett.*, vol. 14, no. 1, pp. 74–76, Jan. 2002.

[16] T. J. Kippenberg, S. M. Spillane, and K. J. Vahala, "Kerr-nonlinearity optical parametric oscillation in an ultrahigh-$Q$ toroid microcavity," *Phys. Rev. Lett.*, vol. 93, p. 083904, Aug. 2004.

[17] J. Moore, M. Tomes, T. Carmon, and M. Jarrahi, "Continuous-wave ultraviolet emission through fourth-harmonic generation in a whispering-gallery resonator," *Opt. Exp.*, vol. 19, no. 24, pp. 24139–24146, Nov. 2011.

[18] T. Carmon, H. Rokhsari, L. Yang, T. J. Kippenberg, and K. J. Vahala, "Temporal behavior of radiation-pressure-induced vibrations of an optical microcavity phonon mode," *Phys. Rev. Lett.*, vol. 94, p. 223902, Jun. 2005.

[19] B. Guha, J. Cardenas, and M. Lipson, "Athermal silicon microring resonators with titanium oxide cladding," *Opt. Exp.*, vol. 21, no. 22, pp. 26557–26563, Nov. 2013.

[20] K. Luke, A. Dutt, C. B. Poitras, and M. Lipson, "Overcoming $Si_3N_4$ film stress limitations for high quality factor ring resonators," *Opt. Exp.*, vol. 21, no. 19, pp. 22829–22833, Sep. 2013.

[21] H. Ou, K. Rottwitt, and H. Philipp, "Novel deep glass etched microring resonators based on silica-on-silicon technology," in *Proc. Integr. Photon. Res. Appl./Nanophoton.*, Uncasville, CT, USA, 2006, paper IMB4.

[22] P. Rabiei, A. Rao, J. Chiles, J. Ma, and S. Fathpour, "Low-loss and high index-contrast tantalum pentoxide microring resonators and grating couplers on silicon substrates," *Opt. Lett.*, vol. 39, no. 18, pp. 5379–5382, Sep. 2014.

[23] C.-Y. Chao and L. J. Guo, "Polymer microring resonators fabricated by nanoimprint technique," *J. Vac. Sci. Technol. B*, vol. 20, no. 6, pp. 2862–2866, 2002.

[24] H. Li, B. Dong, Z. Zhang, H. F. Zhang, and C. Sun, "A transparent broadband ultrasonic detector based on an optical micro-ring resonator for photoacoustic microscopy," *Sci. Rep.*, vol. 4, Mar. 2014, Art. ID 4496.

[25] Y. Zuta, I. Goykhman, B. Desiatov, and U. Levy, "On-chip switching of a silicon nitride micro-ring resonator based on digital microfluidics platform," *Opt. Exp.*, vol. 18, no. 24, pp. 24762–24769, Nov. 2010.

[26] P. Rabiei, W. H. Steier, C. Zhang, and L. R. Dalton, "Polymer micro-ring filters and modulators," *J. Lightw. Technol.*, vol. 20, no. 11, pp. 1968–1975, Nov. 2002.

[27] L.-W. Luo, G. S. Wiederhecker, J. Cardenas, C. Poitras, and M. Lipson, "High quality factor etchless silicon photonic ring resonators," *Opt. Exp.*, vol. 19, no. 7, pp. 6284–6289, Mar. 2011.

[28] J. Cardenas, C. B. Poitras, J. T. Robinson, K. Preston, L. Chen, and M. Lipson, "Low loss etchless silicon photonic waveguides," *Opt. Exp.*, vol. 17, no. 6, pp. 4752–4757, Mar. 2009.

[29] L. J. Guo, "Nanoimprint lithography: Methods and material requirements," *Adv. Mater.*, vol. 19, no. 4, pp. 495–513, 2007.

[30] J. Heebner, R. Grover, and T. A. Ibrahim, *Optical Microresonators: Theory, Fabrication, and Applications*. London, U.K.: Springer-Verlag, 2008.

[31] A. Maxwell, S.-W. Huang, T. Ling, J.-S. Kim, S. Ashkenazi, and L. J. Guo, "Polymer microring resonators for high-frequency ultrasound detection and imaging," *IEEE J. Sel. Topics Quantum Electron.*, vol. 14, no. 1, pp. 191–197, Jan./Feb. 2008.

[32] B. E. A. Saleh and M. C. Teich, *Fundamentals of Photonics*. New York, NY, USA: Wiley, 2007.

[33] C.-Y. Chao, S. Ashkenazi, S.-W. Huang, M. O'Donnell, and L. J. Guo, "High-frequency ultrasound sensors using polymer microring resonators," *IEEE Trans. Ultrason., Ferroelectr., Freq. Control*, vol. 54, no. 5, pp. 957–965, May 2007.

[34] H.-C. Liu, Y.-H. Lin, and W. Hsu, "Sidewall roughness control in advanced silicon etch process," *Microsyst. Technol.*, vol. 10, no. 1, pp. 29–34, Dec. 2003.

[35] C. Zhang, T. Ling, S.-L. Chen, and L. J. Guo, "Ultrabroad bandwidth and highly sensitive optical ultrasonic detector for photoacoustic imaging," *ACS Photon.*, vol. 1, no. 11, pp. 1093–1098, Oct. 2014.

[36] H. Sun *et al.*, "Direct electron beam writing of electro-optic polymer microring resonators," *Opt. Exp.*, vol. 16, no. 9, pp. 6592–6599, Apr. 2008.

[37] X. Lin, T. Ling, H. Subbaraman, L. J. Guo, and R. T. Chen, "Printable thermo-optic polymer switches utilizing imprinting and ink-jet printing," *Opt. Exp.*, vol. 21, no. 2, pp. 2110–2117, Jan. 2013.

[38] Z. Pan *et al.*, "Reconfigurable thermo-optic polymer switch based true-time-delay network utilizing imprinting and inkjet printing," in *Proc. CLEO*, San Jose, CA, USA, 2014, paper SM4G.4.

[39] X. Lin *et al.*, "Ultraviolet imprinting and aligned ink-jet printing for multilayer patterning of electro-optic polymer modulators," *Opt. Lett.*, vol. 38, no. 10, pp. 1597–1599, May 2013.

[40] S.-W. Huang, Y. Hou, S. Ashkenazi, and M. O'Donnell, "High-resolution ultrasonic imaging using an etalon detector array," *Appl. Phys. Lett.*, vol. 93, no. 11, p. 113501, Sep. 2008.

[41] C. Zhang, T. Ling, S.-L. Chen, and L. J. Guo, "Ultra-broad bandwidth ultrasound detector using imprinted polymer microring resonator," in *Proc. CLEO*, San Jose, CA, USA, 2014, p. SM2H.6.

[42] G. J. Diebold, T. Sun, and M. I. Khan, "Photoacoustic monopole radiation in one, two, and three dimensions," *Phys. Rev. Lett.*, vol. 67, pp. 3384–3387, Dec. 1991.

[43] C. Zhang, K. Maslov, J. Yao, and L. V. Wang, "*In vivo* photoacoustic microscopy with 7.6-$\mu$m axial resolution using a commercial 125-MHz ultrasonic transducer," *J. Biomed. Opt.*, vol. 17, no. 11, p. 116016, 2012.

[44] C. Zhang, Y. Zhou, C. Li, and L. V. Wang, "Slow-sound photoacoustic microscopy," *Appl. Phys. Lett.*, vol. 102, no. 16, p. 163702, 2013.

[45] Z. Xie, S.-L. Chen, T. Ling, L. J. Guo, P. L. Carson, and X. Wang, "Pure optical photoacoustic microscopy," *Opt. Exp.*, vol. 19, no. 10, pp. 9027–9034, May 2011.

[46] S.-L. Chen, Z. Xie, T. Ling, L. J. Guo, X. Wei, and X. Wang, "Miniaturized all-optical photoacoustic microscopy based on micro-electromechanical systems mirror scanning," *Opt. Lett.*, vol. 37, no. 20, pp. 4263–4265, Oct. 2012.

[47] S.-L. Chen, T. Ling, and L. J. Guo, "Low-noise small-size microring ultrasonic detectors for high-resolution photoacoustic imaging," *J. Biomed. Opt.*, vol. 16, no. 5, pp. 056001-1–056001-6, 2011.

[48] S.-L. Chen, T. Ling, H. W. Baac, and L. J. Guo, "Photoacoustic endoscopy using polymer microring resonators," *Proc. SPIE*, vol. 7899, pp. 78992T-1–78992T-6, Feb. 2011.

[49] B.-Y. Hsieh, S.-L. Chen, T. Ling, L. J. Guo, and P.-C. Li, "Integrated intravascular ultrasound and photoacoustic imaging scan head," *Opt. Lett.*, vol. 35, no. 17, pp. 2892–2894, Sep. 2010.

[50] B.-Y. Hsieh, S.-L. Chen, T. Ling, L. J. Guo, and P.-C. Li, "All-optical scanhead for ultrasound and photoacoustic dual-modality imaging," *Opt. Exp.*, vol. 20, no. 2, pp. 1588–1596, Jan. 2012.

[51] S.-L. Chen *et al.*, "Efficient real-time detection of terahertz pulse radiation based on photoacoustic conversion by carbon nanotube nanocomposite," *Nature Photon.*, vol. 8, pp. 537–542, May 2014.

[52] S.-L. Chen *et al.*, "Efficient real-time detection of terahertz pulse radiation by 'listening to' photoacoustic generation," in *Proc. Laser Sci.*, Tucson, AZ, USA, 2014, p. LTh4I.1.

[53] E. Z. Y. Zhang and P. C. Beard, "Ultrahigh-sensitivity wideband Fabry–Perot ultrasound sensors as an alternative to piezoelectric PVDF transducers for biomedical photoacoustic detection," *Proc. SPIE*, vol. 5320, pp. 222–229, Jul. 2004.

**Cheng Zhang** received the B.S. degree in electrical engineering from Shandong University, China, in 2010. He is currently pursuing the Ph.D. degree in electrical engineering at the University of Michigan, Ann Arbor, USA. His research interests include polymer-based photonic devices, plasmonics, and metamaterials. He is a Student Member of the Optical Society and the International Society for Optics and Photonics.

**Sung-Liang Chen** received the B.S. degree in electrical engineering and the M.S. degree in electro-optical engineering from National Taiwan University, Taipei, Taiwan, in 2003 and 2005, respectively, and the Ph.D. degree in electrical engineering from the University of Michigan, Ann Arbor, in 2011. He had his post-doctoral training at the University of Michigan Medical School. He is currently an Assistant Professor with the University of Michigan—Shanghai Jiao Tong University Joint Institute, Shanghai, China. His research interests include optical resonators for sensing applications, optical imaging systems, and photoacoustic imaging.

**Tao Ling** received the B.S. degree in physics from Nankai University, China, the M.S. degree in optics from Fudan University, China, and the Ph.D. degree in electrical engineering from the University of Michigan, Ann Arbor, USA. He is currently an Electro-Optical Engineer with TE Connectivity, where he is involved in single mode and multimode transceiver development.

**L. Jay Guo** started his academic career with the University of Michigan in 1999, where he is currently a Professor with the Department of Electrical Engineering and Computer Science. He directs an interdisciplinary laboratory at the intersection of electrical engineering, photonics, polymer materials and mechanical engineering. His group's research includes polymer-based photonic devices and sensor applications, organic and hybrid photovoltaics, plasmonic nanophotonics, and scalable nanomanufacturing technologies, such as roll-to-roll nanoimprinting.